Progress In Electromagnetics Research C, Vol. 114, 69–82, 2021

Multilayer Grid Polarizers: Simulations for Millimeter Waves

Vladimir Yurchenko[1, *], Mehmet Ciydem[2, 3], Marcin Gradziel[4], and Sencer Koc[5]

Abstract—Multilayer grid polarizers for millimeter waves produced with photolithographic technology have been simulated. Polarizers have spectral bands of enhanced performance where polarization extinction ratio in decibels grows in proportion to the number of layers. Full-wave modeling is compared with three asymptotic models for subwavelength gratings using adjusted grating parameters. Random variations of interlayer spacings reduce the enhancement of polarizing performance, yet the latter continues to grow in proportion to the number of layers. Broadband signal detection is also considered.

1. INTRODUCTION

Efficient polarizers are required in many areas ranging from optics to microwaves. Millimeter (MM) and sub-MM wave polarizers operating at the frequencies from 10 GHz to 1 THz are in demand for polarimetric remote sensing [1], radars [2], antennas [3], imaging and spectroscopy [4], security checks [5], etc. Nanowire-grid structures made by the deposition of metallic gratings on dielectric substrates have been developed, which can operate in optics from infrared to ultra-violet bands [6–9]. At the same time, free-standing wire-grid polarizers remain beneficial for MM and sub-MM waves providing minimal absorption and reduced non-polarized reflection [10, 11]. Conventional wire grids suffer, however, from geometrical imperfections, which are increasingly significant in the higher-frequency bands [11].

Improvement of grid polarizers can be achieved through the use of double-layer gratings [12–14]. Ingenious design solutions have been proposed for making stacked or bilayer gratings on different substrates. For double-layer polarizers, exclusion of substrates would also be beneficial.

In 2007, Yurchenko et al. [15] presented free-standing dual-layer wire-grid polarizers for MM wave bands. Experimental testing of these polarizers [16] confirmed a quadratic growth of polarization extinction ratio expressed in relative units as compared to single gratings in the frequency band of 75–110 GHz. Fabrication technology imposed, however, limitations on the performance of gratings in the higher frequency bands, i.e., for THz (sub-MM) waves.

An alternative design utilizes the chemical etching of metallic gratings on ultra-thin polymer films. An attempt of making the polarizers of this kind was described in Ref. [17]. Other kinds of advanced polarizers have been developed later [18–26]. They include bilayer and dual-bilayer structures on flexible or rigid substrates fabricated, mostly, for infrared and THz applications. Bilayer structures are, typically, the systems with subwavelength distance between gratings [14]. This makes broadband polarizers of high performance, though it is slightly lower than the performance of structures operating in the resonant mode. At the same time, substrates introduce additional losses, which can be avoided in the MM and near sub-MM wave bands where gratings with no substrates can be made.

In this publication, we propose multilayer grid polarizers assembled of purely metallic gratings. The structures are free-standing (free of lossy reflective dielectric substrates) quasioptical polarizers for MM waves (assemblies operating at the frequencies $f = 10$–250 GHz) that have been fabricated with conventional sub-MM-scale photolithographic technology.

Received 11 March 2021, Accepted 8 July 2021, Scheduled 21 July 2021

* Corresponding author: Vladimir Yurchenko (v.yurchenko.nuim@gmail.com).

[1] TUBITAK 2221 Fellowship Program, Electrical and Electronics Engineering Department, Middle East Technical University, Ankara, Turkey. [2] Electrical and Electronics Engineering Department, Gazi University, Ankara, Turkey. [3] Engitek Engineering Technologies Ltd, Ankara, Turkey. [4] Maynooth University Department of Experimental Physics, Maynooth, Ireland. [5] Electrical and Electronics Engineering Department, Middle East Technical University, Ankara, Turkey.

2. MULTILAYER POLARIZER MODEL

Schematics of a free-standing multilayer polarizer and a single grating fabricated by photolithographic technology are shown in Figure 1. The polarizer is made as a tandem of n planar metallic gratings, which are orthogonal to the x axis and separated one from another by spacers of thickness b. Each grating is specified by the period p, with conductive strips of width w and thickness t parallel to the z axis. The incident uniform plane wave is assumed to propagate in the positive direction of the x axis.

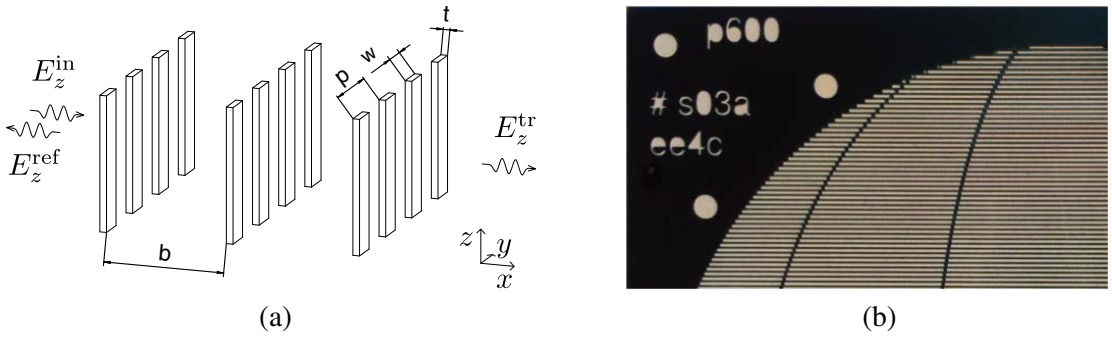

Figure 1. (a) Schematics of a multilayer grid polarizer and (b) a single grating for multilayer assembly.

For the experiments, a few kinds of brass gratings have been produced as specified by the parameters $p = 0.60\,\text{mm}$, $w = 0.17\,\text{mm}$, $t = 0.10\,\text{mm}$, $b = 6.00\,\text{mm}$, and the aperture diameter $D = 100\,\text{mm}$. For reinforcement of grating structures, some strengthening elements were introduced in the design, e.g., a few transverse cross-strips as shown in Figure 1(b), quasi-random point-like cross-links instead of continuous cross-strips, and other solutions. In simulations, wire gratings have also been considered where conductive strips of rectangular cross-section are replaced by cylindrical wires of the diameter w. The air spacers between wire gratings are also defined by the parameter b.

The polarizers assembled of $n = 1$, 2, 3, and 4 gratings have been prepared for experimental testing in the MM-wave bands. The testing is going to be made in the frequency band of $f = 20$–$40\,\text{GHz}$ at the Electrical and Electronics Engineering Department, Middle East Technical University, Ankara, Turkey, and in the band of $f = 75$–$110\,\text{GHz}$ at the Maynooth University Experimental Physics Department, Maynooth, Ireland, where the relevant experimental facilities have been developed.

The aim of this work is the computer simulation of multilayer grid polarizers in the broad frequency range of $f = 10$–$250\,\text{GHz}$ for optimization of their design and prediction of polarizer performance with account of some imperfections of gratings and limitations imposed by applications. The research is focused on the performance of gratings needed for applications rather than on simulation methods, of which a great variety is available [27, 28].

Innovations include the proposal for making MM-wave polarizers as multilayer stacks of free-standing metallic gratings produced by photolithographic technology, simulations of multilayer gratings by a series of exact and asymptotic methods with criss-cross comparison of solutions, a procedure for producing nearly exact results with asymptotic methods via adjusting the model parameters, and estimates of the effects of imperfections in multilayer structures. A formulation has been proposed that makes the finite-element method designed for the closed domains to become suitable for the given kind of an open domain problem as well. The benefits of multilayer polarizers are their enhanced performance at rather coarse and robust design, easy fabrication and, potentially, an extended area of applications.

3. ACCURATE FULL-WAVE SIMULATIONS

Full-wave simulations of multilayer gratings were made with FlexPDE software [29]. The software is designed for solving partial differential equations with finite element method. For the electromagnetic scattering problems, the method requires the Helmholtz equation to be written in the gradient form. Here we develop our formulations in a way as we explained earlier [30].

For doing simulations, one has to specify the model parameters (geometry and material properties of the device components), processing parameters (number of iterations, required accuracy, etc.), governing equations, and boundary conditions. Boundary conditions are imposed with standard operators, which set the values of either the unknown functions or their derivatives normal to the boundary. No access to internal equations and their processing other than specified above is provided. The output of simulations is a solution in both the graphical and digital forms that can be used for further analysis.

At the given geometry of gratings, the simulation model is simplified. In this case, the scattering problem is two-dimensional where the fields depend on spatial coordinates x and y.

In the case of E polarization, the incident wave has the electric field $\vec{E}^{in}$ parallel to the z axis (see Figure 1), and the Helmholtz equation in the free space surrounding the gratings takes on the form

$$\nabla\left(\mu^{-1}\nabla\left(E_z\right)\right) + k_0^2\varepsilon E_z = 0 \tag{1}$$

where E_z is the complex amplitude of z component of the total electric field $\vec{E}$; $k_0 = \omega/c$ is the free-space wavenumber, $\omega = 2\pi f$; c is the free-space speed of light; $\mu = 1$ and $\varepsilon = 1$ are the relative permeability and permittivity of the free space, and the oscillatory time-dependence $\exp(-i\omega t)$ is assumed. The boundary condition $E_z = 0$ is imposed at the strip (wire) surfaces assuming that the strips (wires) are perfect electrical conductor (PEC) materials.

In the case of H polarization, the magnetic field $\vec{H}$ replaces $\vec{E}$; the quantities μ and ε replace each other; and the boundary condition at the strip (wire) surfaces takes on the form $\partial H_z/\partial\hat{n} = 0$ where $\hat{n}$ is the unit normal to the surface of every strip (wire) in the domain.

The incident wave is introduced via the boundary condition, which is imposed on either the E_z or H_z component, depending on polarization, at the front surface of computation domain ahead of the grating structure ($x = X_L$). The boundary condition requires the incident wave of unit amplitude to enter the domain through the surface. At the same time, any waves are allowed to leave the domain with no obstruction. In a similar way, the radiation condition is imposed at the rear surface behind the structure ($x = X_R$) where no incoming wave should enter the domain [30]. The conditions at the side borders are defined at $y = \pm Y_s$ in a symmetric manner assuming that an integer number of grating periods are included in the domain, and no waves propagate across the borders.

Specifically, the side border conditions for, e.g., the E_z field take on the form

$$\partial E_z/\partial y = 0 \quad \text{at} \quad y = \pm Y_s \tag{2}$$

when the borders $y = \pm Y_s$ are chosen to cross the centers of air slots or metal strips of subwavelength gratings where, due to the symmetry, the extrema occur for the fields as the functions of y.

The radiation conditions at the front and rear surfaces of the domain require more preparations. The latter are based on the fact that the fields away from subwavelength gratings take on the form of propagating plane waves. This form is acquired at the distance greater than a few periods of subwavelength grating that could be much smaller than the radiation wavelength λ.

Thus, at the borders $x = X_R$ and $x = X_L$ placed at the distance of about one λ from gratings, the transmitted and reflected wave fields take on the form $E_z^{tr} = T^E \exp(ik_0 x)$ and $E_z^{ref} = R^E \exp(-ik_0 x)$, respectively, where T^E and R^E are the unknown transmission and reflection coefficients, i.e., the S_{21}^E and S_{11}^E elements of scattering matrix $\hat{S}^E$ that have to be found. The total fields at the relevant borders are $E_z = E_z^{tr}$ and $E_z = E_z^{ref} + E_{z0}^{in}\exp(ik_0 x)$ where E_{z0}^{in} is the given amplitude of the incident wave ($E_{z0}^{in} = 1$). In terms of the total field, the radiation conditions take on the form

$$\partial E_z/\partial x - ik_0 E_z = 0 \qquad \text{at} \quad x = X_R\ , \tag{3}$$

$$\partial E_z/\partial x + ik_0 E_z = 2ik_0 E_{z0}^{in}\exp(ik_0 x) \qquad \text{at} \quad x = X_L\ . \tag{4}$$

In this form, they are explicitly implemented with standard FlexPDE operators. This makes the set of boundary and radiation conditions complete in the framework of the FlexPDE software and suitable for generating solutions to the given problem in the domain of parameters being of interest.

The quantities of interest are the transmitted and reflected waves of E and H polarizations defined at the surfaces $x = X_R$ and $x = X_L$, respectively. Below we consider E_z^{tr} components of transmitted waves of E polarization, which is the rejected polarization in the transmission. We simulate transmission spectra $E_z^{tr}(f)$ of E polarized waves propagating through multilayer gratings at the frequencies ranging

from $f = 10\,\text{GHz}$ to $f = 250\,\text{GHz}$. The waves of H polarization are transmitted through the given structures with negligible reflection that makes the E_z^{tr} spectra sufficiently good representatives of polarization extinction ratio of polarizers being considered.

An example of two solutions for the E_z field distribution in a two-layer grid structure is shown in Figure 2. The field is computed at the frequencies (a) $f = 24.5\,\text{GHz}$ and (b) $f = 24.7\,\text{GHz}$, both being close to the first resonant frequency $f_{p1} = 24.4787\,\text{GHz}$. The latter is observed when the half-wavelength $\lambda/2 = 6.124\,\text{mm}$ matches the distance $b + t = 6.100\,\text{mm}$ between the center planes of two gratings.

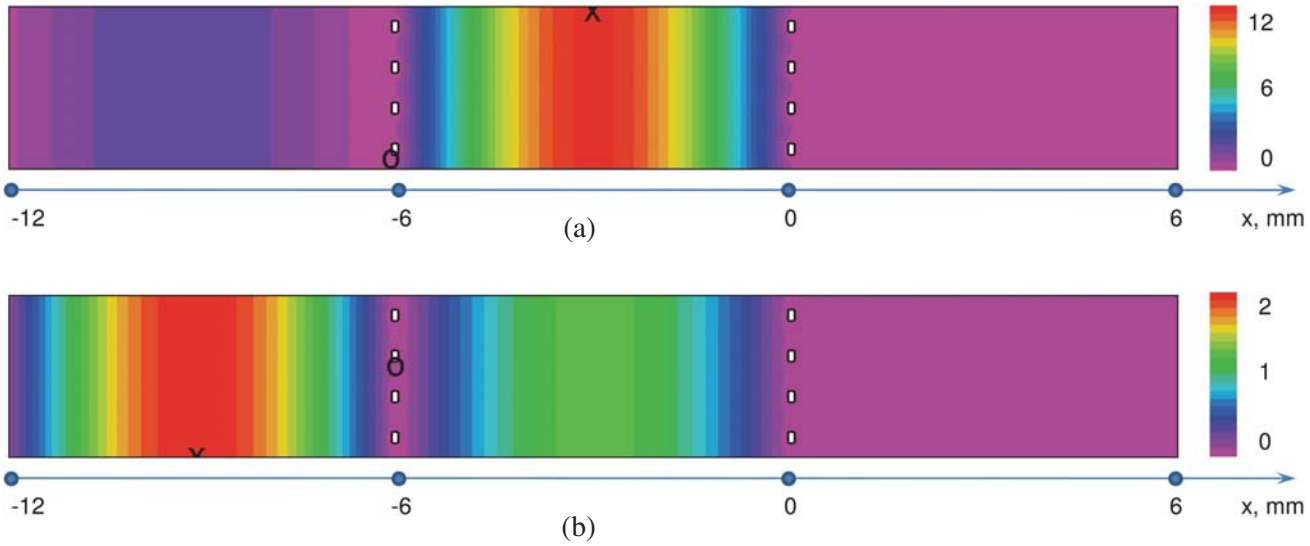

Figure 2. The amplitude of simulated $E_z(x, y)$ field component in a two-layer grid structure G_2 with interlayer spacing $b = 6.00\,\text{mm}$ at the frequency (a) $f = 24.5\,\text{GHz}$ and (b) $f = 24.7\,\text{GHz}$ (the case of rejected polarization near the first resonant transmission peak frequency $f_{p1} = 24.4787\,\text{GHz}$, symbols "o" and "x" on the plot show the locations of minima and maxima).

Transmission and reflection at the frequencies $f = 24.5$ and $24.7\,\text{GHz}$ are found to be $P_{tr} = -12.95$ and $-32.90\,\text{dB}$ and $P_{ref} = -0.238$ and $-0.002\,\text{dB}$, respectively. This compares with $P_{tr} = -0.214\,\text{dB}$ and $P_{ref} = -31.76\,\text{dB}$ at the resonant frequency $f_{p1} = 24.4787\,\text{GHz}$. Transmission is invisible in Figure 2, though it appears at the resonance. Reflection is significant and leads to the formation of standing waves in front of the structure.

At a closer look, one can see minor field variations along the gratings. They show a limited wave transmission through narrow slots in subwavelength gratings, though transmission increases at the resonant frequency. The field variations are localized in a narrow zone at the grating surface. The zone thickness is about one grating period, which is much smaller than the wavelength in the case of a subwavelength grating.

Approaching the resonant frequency, the field increases in a cavity between gratings as a result of multiple reflections under the conditions of constructive interference. In the given example, the field between gratings surpasses the amplitude of the incident wave at the exact resonance up to 55 times. This increases the transmission of the waves of rejected polarization, which is a negative effect of multigrid structures.

Transmission spectra of E_z^{tr} field component are presented in Figure 3. The spectra show the bandwise operation of multilayer grid polarizers arising due to the resonant effects.

With increasing the number of gratings in a multilayer assembly, polarization extinction ratio defined as the ratio of transmittance of the waves of allowed and rejected polarizations, respectively, in the rejection frequency bands increases in decibels approximately in proportion to the number of layers. At the same time, minibands of resonant transmission of gradually increasing bandwidth are formed in the transmission spectrum for the waves of rejected polarization. The minibands appear due

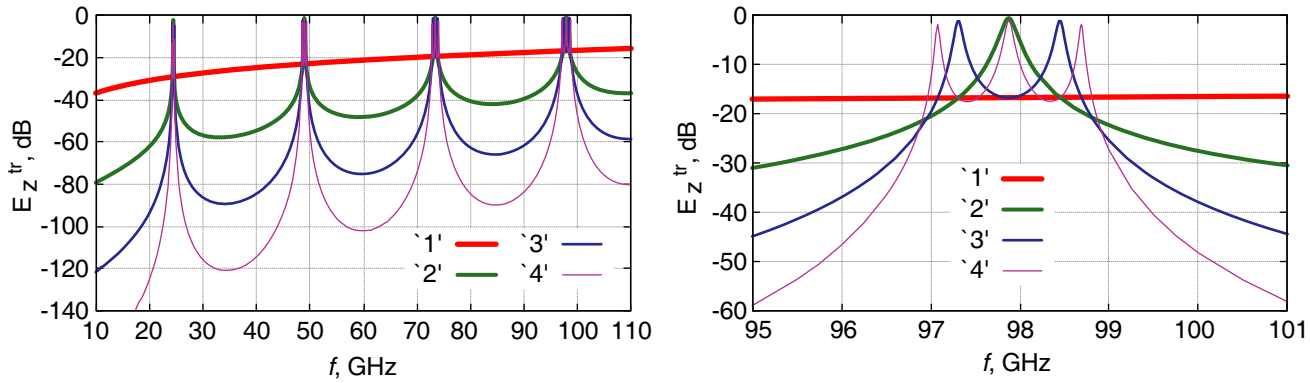

Figure 3. Full-wave simulated transmission spectra of E_z^{tr} field component (a) in the band of $f = 10 - 110$ GHz and (b) at the 4th-order resonant transmission peak (p_4) for the assemblies G_n of $n = 1, 2, 3, 4$ gratings presented in Figure 1 with interlayer spacings $b = 6.00$ mm (rejected polarization, curves '1' to '4', respectively).

to the multiple mode splitting of resonant field oscillations excited in the cavities between gratings in a multilayer assembly.

It is instructive to have a look at the field distributions in the structures at the resonant frequencies. In a three-layer structure, at the first resonant transmission of rejected polarization (p_1 peak), the field oscillates at maximum amplitude in both minicavities between the adjacent gratings that causes the enhanced transmission. Mode splitting occurs due to weak coupling between cavities that results in the doublet peak splitting. At the lower peak frequency $f_{p_1}^{(1)} = 24.341$ GHz, the field in both the cavities oscillates in phase. At the higher frequency $f_{p_1}^{(2)} = 24.618$ GHz, the field oscillates in counter-phase.

A more intricate process happens in the four-layer structure where triplet peak splitting occurs. Figure 4 shows the field amplitude and phase distributions in the structure at the 2nd-order triple-split transmission peak (p_2) of E polarized plane wave. The distributions are computed at the very tips of triple-split peak transmission, which occur at the frequencies $f_{p_2}^{(k)} = 48.563$, 48.953, and 49.351 GHz for each sub-peak $k = 1, 2, 3$ (curves 1 to 3, respectively).

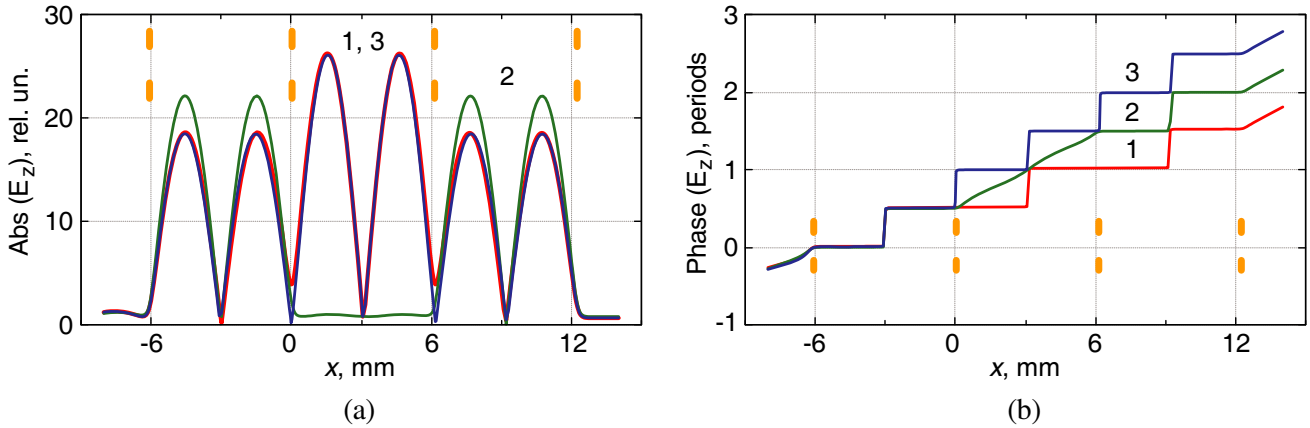

Figure 4. (a) Amplitude and (b) phase of E_z field component of plane wave propagating through a 4-layer grating structure G_4 (dash lines show locations of gratings) at the resonant frequencies $f_{p_2}^{(k)}$ of triple-split 2nd-order transmission peak p_2 (see curve '4' in Figure 3) where $f_{p_2}^{(k)} = 48.563$, 48.953, 49.351 GHz ($k = 1, 2, 3$, curves 1 to 3, respectively).

In this case, at the 1st and 3rd sub-peaks of transmission, the field oscillates at maximum amplitude in the middle cavity and has lower amplitudes in the two external cavities (at the 2nd-order peaks, minicavities are of two half-wavelength size). At the 2nd sub-peak, however, the field oscillates in the external cavities only, being of the same amplitudes, while the resonance in the middle cavity is damped. At the same time, the phase of oscillations increases through the structure in steps in such a way that when progressing from the 1st to the 3rd sub-peaks of triple-split resonant transmission, the phase at every sub-peak acquires an extra step increase by half-oscillation period.

4. APPROXIMATE ASYMPTOTIC SOLUTIONS

Full-wave FlexPDE solutions to the given problem can be obtained up to the frequency of 250 GHz when the wavelength is reduced to twice the period of gratings, and simulations fail. In general, full-wave simulations are time-consuming and lose convergence with increasing the frequency and the number of gratings. So, much faster approximate solutions are in demand for practical applications. Comparison of exact and approximate solutions is a useful step in the choice of simulation method. Here we compare full-wave FlexPDE simulations with approximate models for multilayer structures that use (1) generic asymptotic Wainstein solution for S-matrix of subwavelength zero-thickness strip gratings [31] ('gs' solution), (2) similar Wainstein solution for cylindrical wire gratings [31] ('gw' solution), and (3) regularization-based solution for strip gratings [28, 32–34] ('gr' solution [17] that in the case of subwavelength gratings is expected to be similar to the 'gs' solution above).

Simulation parameters which have to be used for obtaining specific equivalent asymptotic models ('s', 'w', 'r' models, respectively) at the given grating period $p = 0.60$ mm, i.e., the parameters providing a good fit to FlexPDE solutions in Figure 3 computed above at $t = 0.10$ mm, $w = 0.17$ mm, and $b = 6.00$ mm, are found to be

(1) 's' model: $w = 0.29$ mm and $b = 6.06$ mm ($t = 0$ mm),
(2) 'w' model: $w = 0.15$ mm and $b = 6.12$ mm, and
(3) 'r' model: the same as defined for 's' model above.

For the wire gratings, generic asymptotic 'gw' solutions coincide with full-wave simulations at the same parameters of subwavelength structures, though they deviate gradually from exact solutions when the wavelength decreases towards the grating period. For strip gratings, both the Wainstein 'gs' and regularization-based 'gr' models ($t = 0$) also coincide with full-wave solutions for subwavelength multilayer gratings at the same parameters when the strip thickness t is sufficiently small. For gratings of period $p = 0.60$ mm and strip width $w = 0.17$ mm, a suitable thickness is $t < 0.01$ mm.

The actual gratings, though not being wire grids, have quite significant thickness $t = 0.10$ mm comparable to the strip width $w = 0.17$ mm. This makes the real gratings less transparent for the E polarized waves than small-thickness PEC strip gratings at the same p and w values and, at the same time, slightly more transparent than wire gratings at the given value of $w = 0.17$ mm as the wire diameter (Figure 5). So, the effective parameters of equivalent 's', 'w', and 'r' models have to be properly adjusted for providing a good fit to full-wave solutions for real gratings as explained above.

Figure 6(a) shows a good match between the full-wave FlexPDE and the equivalent 's' model solutions for strip gratings of $n = 1$, 2, and 3 layers. It also indicates that FlexPDE simulations fail to converge for the three-layer structure at the frequencies above $f = 190$ GHz where the asymptotic solution can be used as an acceptable approximation. Figure 6(b) presents the transmission spectra computed for strip grating multilayer structures with equivalent 'w' and 'r' simulation models. It shows a remarkable similarity of results obtained with essentially different asymptotic approximations.

Thus, numerical models based on asymptotic solutions for subwavelength gratings when using adjusted values of grating parameters provide sufficiently accurate and efficient simulation tools for the analysis of multilayer polarizer structures.

A few comments about the characteristics and implementation of asymptotic solutions can be added. All asymptotic methods are approximate. At the same time, the solutions presented above are remarkably accurate. The reason is that asymptotic solutions utilize advanced approximations and properly evaluate the resonant response of multilayer assemblies.

In the models above, the structure response is found numerically by computing the transmission matrix $\hat{M}_{m,0}^{E(H)}$, depending on polarization, which defines the connection between the electric and

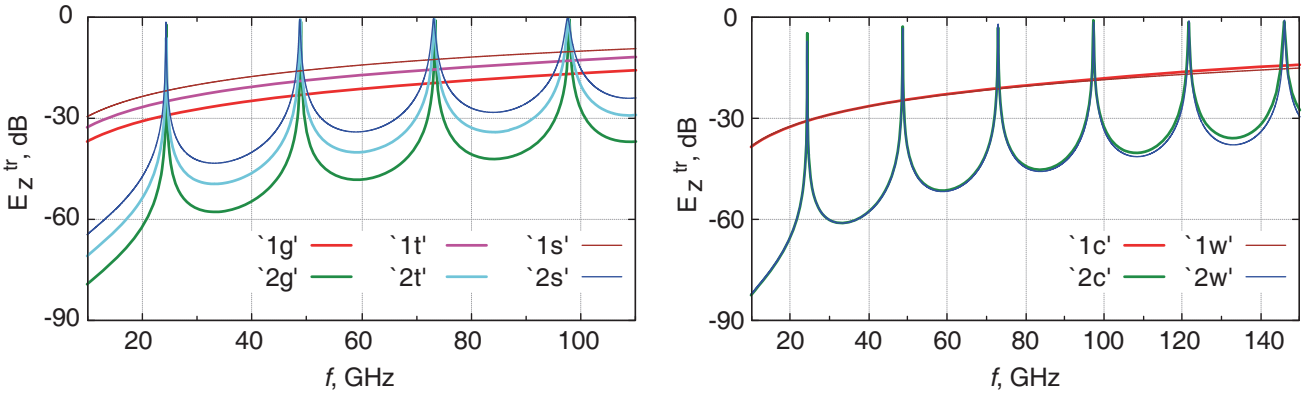

Figure 5. (a) FlexPDE vs asymptotic solutions for G_n ($n = 1, 2$) multilayer gratings of (a) strips of width $w = 0.17\,\text{mm}$ and thickness $t = 0.10\,\text{mm}$ and $0.04\,\text{mm}$ (FlexPDE, curves with suffix 'g' and 't', respectively), and $t = 0\,\text{mm}$ ('gs' solutions, curves with suffix 's'), and (b) wires of the diameter $w = 0.17\,\text{mm}$ (FlexPDE and 'gw' solutions, curves with suffix 'c' and 'w', respectively).

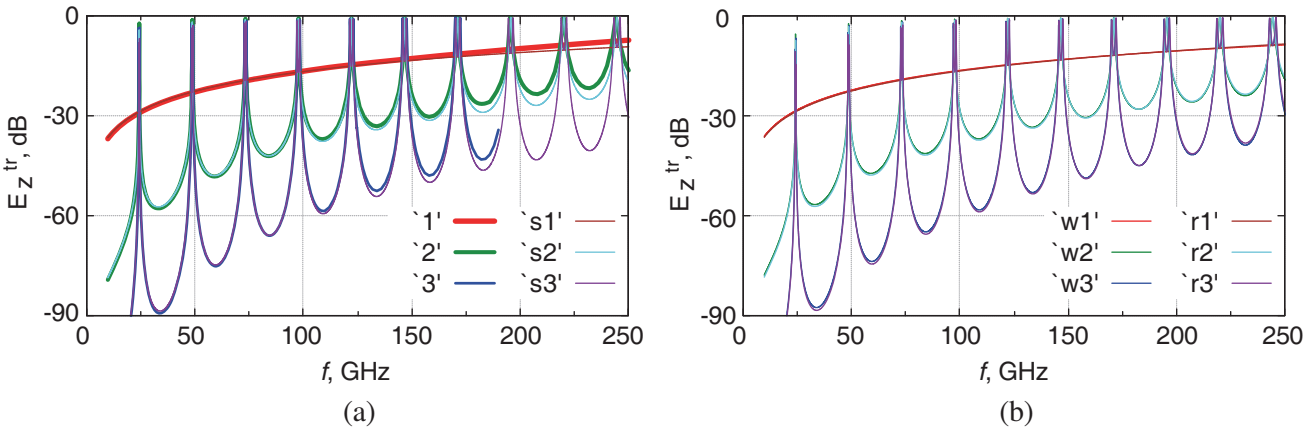

Figure 6. (a) Full-wave FlexPDE vs 's' model asymptotic solutions for strip grating G_n structures (curves '1' to '3' vs 's1' to 's3', $n = 1, 2, 3$, respectively) and (b) 'w' model asymptotic solutions vs regularization-based 'r' model results (curves 'w1' to 'w3' vs 'r1' to 'r3', respectively).

magnetic fields on the opposite sides of structure as, e.g., in the case of E polarization

$$\{E_{z_m}, H_{y_m}\} = \hat{M}^E_{m,0} \cdot \{E_{z_0}, H_{y_0}\} \tag{5}$$

where the indices m and 0 point to the left- and right-hand sides, respectively, of the multilayer structure when the latter is considered as a stack of m slices, each being either the grating or the space between gratings. $\{\,.\,,\,.\,\}$ means the column vector, and $\hat{M}^E_{m,0}$ is the 2×2 transmission matrix of the stack [35]. The matrix $\hat{M}^E_{m,0}$ is computed as a product of matrices $\hat{M}^E_{j,(j-1)}$ of separate slices $j = 1, \ldots, m$

$$\hat{M}^E_{m,0} = \hat{M}^E_{m,(m-1)}\ \hat{M}^E_{(m-1),(m-2)}\ \ldots\ \hat{M}^E_{1,0}. \tag{6}$$

Should the matrices $\hat{M}^E_{j,(j-1)}$ deliver exact solutions and the plane-wave model be precise, a solution would be exact. In this ways, $\hat{M}^E_{m,0}$ precisely evaluates the resonances specific to the structure.

For subwavelength gratings, when $p \ll b$, the fields at the opposite sides of each slice, being linked by matrices $\hat{M}^E_{j,(j-1)}$, should be defined slightly away from gratings at the distance of about p where all

the waves turn into plane waves. These are the fields, for which the asymptotic solutions in Ref. [31] had been found. The solutions provide the reflection and transmission coefficients $R_k^{E(H)}$ and $T_k^{E(H)}$ of a single grating k as presented in Ref. [31] by Eqs. (2.30) and (2.31) for the cases of E and H polarizations, respectively. The parameters are defined by a series of other equations depending on the kind of gratings and values of λ, grating period p, and strip width or wire diameter w, thus, providing asymptotic solutions for separate gratings in the 'gs' and 'gw' models.

For the 'gr' model, Chapter 2 in Ref. [28] delivers formulations for the exact numerical solution of grating problems that had been implemented in relevant software earlier and utilized here for generating the $R_k^{E(H)}$ and $T_k^{E(H)}$ asymptotic coefficients of subwavelength gratings.

The scattering matrices of single gratings defined by coefficients R_k^E and T_k^E (considering again the case of E polarization) can eagerly be converted into the transmission matrices $\hat{M}^E_{j,(j-1)}$. After defining similar matrices for air spaces and multiplying all the matrices according to Eq. (6), we obtain the final matrix $\hat{M}^E_{m,0}$. Then, converting the transmission matrix $\hat{M}^E_{m,0}$ into the scattering matrix $\hat{S}^E$, we compute the reflection R^E and transmission T^E coefficients of any multigrid structure assembled of subwavelength gratings.

We used the technique based on Eq. (6) for simulation of multilayer gratings at the plane wave incidence [15–17] and, with an extension for generic stratified media and arbitrary beams, applied it to dielectric structures [36–38]. Available experiments confirm the validity of this technique [16, 36–38].

5. POLARIZING EFFICIENCY WITH BROADBAND DETECTION

Multilayer polarizers could be used in any frequency bands ranging from optics to microwaves. In optics, infrared, and THz bands, the interlayer spacers in polarizers could be of macroscopic size, being large as compared to the wavelength. This makes the frequency bands between the transmission peaks relatively small. At the same time, both the excitation sources and the detectors utilized in various applications could largely be broadband such as the bolometric detectors. This requires the analysis of polarizer response with account of broadband signal detection. Here we simulate the polarizer transmission signal as recorded with a model detector specified by the spectral sensitivity curve $S(f)$.

Figure 7 shows the transmission spectra E_z^{tr} computed for multilayer grating assemblies G_n ($n = 1$, 2, 3) with asymptotic 'w' simulation model (wire grating approximation) assuming the spectra to be measured with monochromatic (curves 'w1' to 'w3') and broadband, e.g., bolometric detector (curves 'b1' to 'b3', respectively). The spectral sensitivity of broadband detector is defined by the function $S(f) = S_0 \cos^2(\pi f/2\delta f)$ at $|f| \le \delta f$ and $S(f) = 0$ at $|f| > \delta f$ where δf is the full bandwidth at half-magnitude sensitivity and $S_0 = 1/\delta f$. In this case, the total spectral range of sensitivity is $\Delta f = 2\delta f$, and the total sensitivity $S_t = \int_{-\infty}^{\infty} S(f)df$ is normalized to $S_t = 1$.

The transmission spectrum measured by broadband incoherent (bolometric) detector, when being presented as the effective field $E_z^{tr}(f)$ corresponding to the bandwidth-average power registered by the detector, is computed as

$$E_z^{tr}(f) = \left(\int_{-\infty}^{\infty} \left| \tilde{E}_z^{tr}(f') \right|^2 S(f - f')df' \right)^{1/2} \tag{7}$$

where $\tilde{E}_z^{tr}(f')$ is the actual complex amplitude of monochromatic plane wave transmitted through the structure at the frequency f'.

Curves 'b1' to 'b3' in Figures 7(a) and (b) computed according to these definitions present the spectra that would be measured with the detector of half-magnitude bandwidth (a) $\delta f = 5\,\mathrm{GHz}$ and (b) $\delta f = 20\,\mathrm{GHz}$, respectively. The curves show that transmission spectra of rejected polarization obtained with multilayer gratings, when being measured with small yet non-zero bandwidth, have their resonant peaks broadened and reduced to the level of signal transmitted by a single-layer grating. At the same time, low-transmission valleys between the peaks remain unchanged, as deep as measured with a monochromatic detector, and decrease in decibels in proportion to the number of gratings in the assembly.

When measured with a detector of large bandwidth δf, which is comparable to the inter-peak spacing Δf_p defined by the grating interlayer distance b as $\Delta f_p = c/2b$, the periodic modulation of

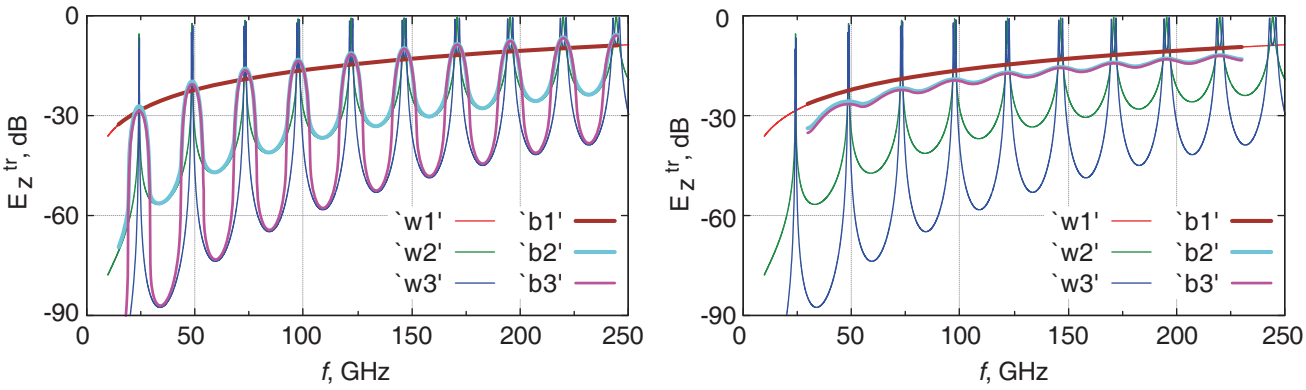

Figure 7. Transmission spectra E_z^{tr} computed for the wire-grid assemblies G_n ($n = 1, 2, 3$) if measured with monochromatic (curves 'w1' to 'w3') and broadband detector (curves 'b1' to 'b3', respectively) at the detector bandwidth (a) $\delta f = 5\,\text{GHz}$ and (b) $\delta f = 20\,\text{GHz}$.

spectra of multilayer structures almost disappears, and the polarizer performance is not improved with increasing the number of gratings, remaining nearly the same as the one of a single-layer structure.

6. POLARIZER WITH VARYING INTERLAYER SPACINGS

Another essential effect in multilayer structures is the random variation of interlayer spacings. The latter may be of two kinds. In one case, the gratings may remain flat and parallel to each other, but spacings between different gratings would differ one from another. In the other case, the gratings may lose their flatness and acquire some roughness on the polarizer aperture. Both the effects would smear the resonant peaks in the transmission spectra, but the benefits of multilayer arrangement may also disappear.

For the analysis of the effect, we assume that the variations of spacings b are small and smooth as functions of transverse coordinates over the polarizer aperture. This allows us to neglect a small effect of wave scattering and consider only the local phase variations of the transmitted waves. When the transmitted wave is registered by the receiver behind the polarizer, the total signal recorded by the detector is defined by the average value of the complex field amplitude over the aperture, thus, making the relevant averaging of the local wave contributions with account of phases.

For quantitative evaluation, we use a Gaussian distribution of deviations δx_k of grating surface from an ideal position over different "pixel patches" across the aperture of each grating at standard deviation σ, thus, introducing local variations δb_k of spacings b. The scales of variations over transverse y and z coordinates should be large whereas deviations δb_k should be small. We use a set of K values δx_k for each grating and generate n different sets for the modeling of an n-layer structure G_n. The estimates of transmission spectra computed in this model are shown in Figures 8 and 9.

Figure 8(a) shows the transmission spectra at the 5-th order resonant transmission peak for the strip-grating assemblies G_n of $n = 1$ to 4 layers at the value of $K = 3$ ($\sigma = 0.15\,\text{mm}$). The signal E_z^{tr} is obtained as a coherent summation of fields transmitted through K samples of each structure with slightly different spacings b of different gratings in different samples. As a result, the main transmission peak undergoes splitting in $(n-1)K$ resonant subpeaks at random frequencies, which could partially overlap. If $K = 1$, we obtain structures of perfectly flat gratings with small variations of spacings. They show transmission peak splitting in $n-1$ subpeaks similar to those in Figure 3(b), though emerging at slightly random frequency of each subpeak.

The effect of resonant peak splitting into multitude of subpeaks at large values of K leads to smearing off the transmission peaks of multilayer structures with uneven grating surfaces. The effect is clearly seen in Figure 8(b) which shows the transmission spectra of the same G_n structures computed at $K = 900$. The varying spacings are assigned to random "pixel patches" across the aperture so

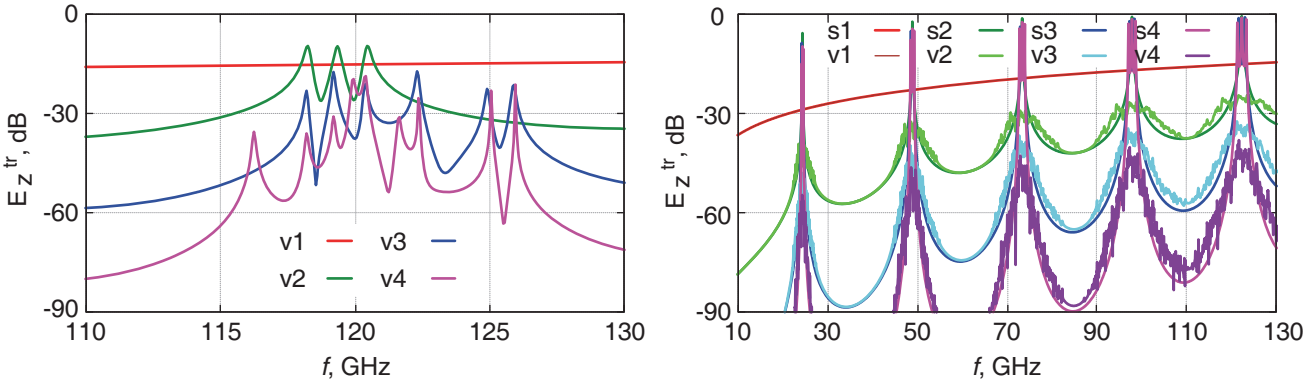

Figure 8. Transmission spectra of the waves of E_z polarization computed for strip-grating assemblies G_n of $n = 1$ to 4 layers with roughness of gratings specified by Gaussian distribution with standard deviation $\sigma = 0.15\,\text{mm}$ using the random sampling of (a) $K = 3$ and (b) $K = 900$ "pixel patches" as compared to the ideal case of $\sigma = 0$ ('s' model, curves 'v1' to 'v4' vs 's1' to 's4', respectively).

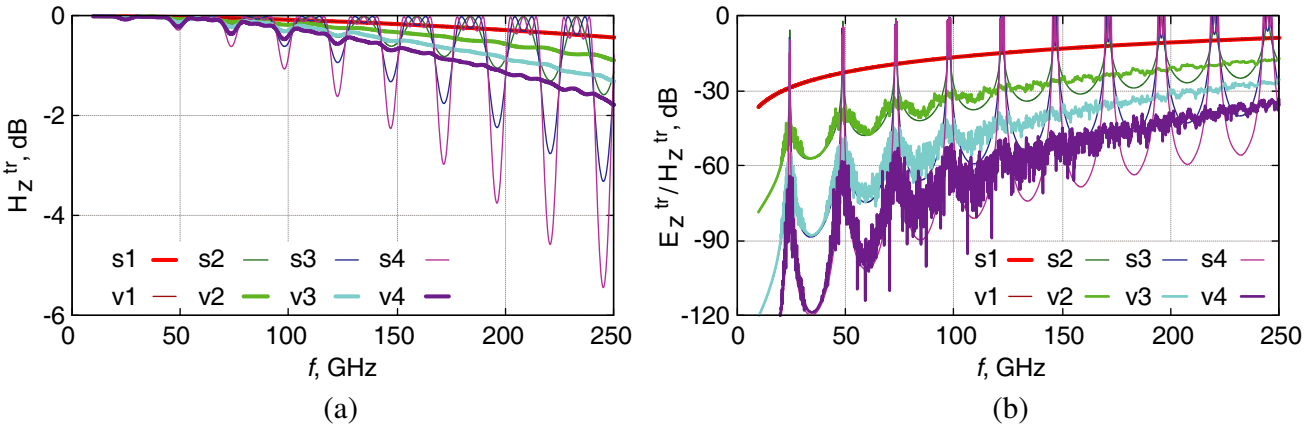

Figure 9. (a) Transmission spectra of the waves of H_z polarization and (b) polarization extinction ratio E_z/H_z computed for strip-grating assemblies G_n of $n = 1$ to 4 layers in the model with roughness of gratings specified by parameters $\sigma = 0.3\,\text{mm}$ and $K = 900$ as compared to the ideal case of gratings at $\sigma = 0$ ('s' model, curves 'v1' to 'v4' vs 's1' to 's4', respectively).

that the size of patches is large as compared to the radiation wavelength λ and small as compared to the aperture size D. If choosing the aperture size $D = 300\,\text{mm}$, the patch diameter would be about $d = 10\,\text{mm}$, which is greater than both the grating period $p = 0.6\,\text{mm}$ and the wavelength $\lambda = 3\,\text{mm}$ at the typical frequency $f = 100\,\text{GHz}$ whereas local grating deviations from an ideal position is in the range of $|\delta x_k| < 0.5\,\text{mm}$ at $\sigma = 0.15\,\text{mm}$.

Random variations of resonant frequencies across the aperture lead to the cut-off and broadening of total transmission peaks for the waves of rejected E_z polarization as compared to the case of an ideal multilayer structure. The peaks acquire random profile and noticeable broadening even at low level of variations, e.g., at the values of $\sigma = 0.15\,\text{mm}$ and $\lambda = 12\,\text{mm}$ ($f = 25\,\text{GHz}$). Here, σ is by two orders of magnitude smaller than λ, being also smaller than subwavelength grating period p.

When the magnitude of variations increases, the valleys of low transmission between the resonant peaks also acquire random profile and raise closer to the level of a single grating transmission, though, for multilayer gratings, the level of rejected polarization remains lower than the transmission level of single gratings. Reduced transmission of rejected polarization by multilayer structures with random

roughness of gratings continues to decrease with increasing the number of grating layers, though the rate of reduction is smaller than the one observed in the ideal structures.

Roughness of gratings affects the transmission of waves of allowed polarization also, see Figure 9(a) (here, $\sigma = 0.3\,\text{mm}$). In this case, resonances are also smeared, and transmission decreases gradually with increasing the frequency, though the loss of transmission is small at the given structure parameters. As a result, the ratio E_z^{tr}/H_z^{tr} increases faster with increasing the frequency than the transmission signal E_z^{tr}, see Figure 9(b).

The given estimate of roughness effect is simplistic. It does not account for the diffraction and presents the wavefronts as step-wise random surfaces. Yet, it is the random shape of wavefronts that makes the conditions of constructive interference rapidly vary when sweeping the frequency. This causes a random rippling (noisy profile) to appear on transmission and reflection spectra, which is typical for multilayer structures with random rough interfaces [39].

At the same time, the effect of multiple reflections between gratings has been accounted for. The effects of imperfections reducing the wave coherence rapidly accumulate with increasing number of gratings. When a new grating is added, additional scattering emerges between the new grating and the other ones. As a result, the coherence drops even faster with addition of every next grating. Therefore, the performance of a multilayer polarizer is getting limited at a certain number of layers by insufficient quality of gratings in use.

The approximation neglecting the wave diffraction is justified at small distances from random screens characterized by small roughness [40]. The condition would be valid for small interlayer spaces ($b \sim \lambda$) in structures with relatively smooth gratings. Yet, the approximation may have to be replaced with a better one at the resonant frequencies. The validity of the model may also degrade with increasing the number of gratings because of increasing significance of multiple scattering.

Noisy profiles of transmission spectra obtained in our model resemble experimental curves measured with various bilayer and dual-bilayer gratings [12, 20–23]. Steady increase of noise with increasing the frequency is observed for gratings made by nanoimprinting method [20] which could be caused by significant imperfections of these gratings. Huang et al. [21] provided experimental proof that noisy spectra appear due to imperfections of structures rather than measurement system. Our simulations indicate that noisy profiles could appear as a result of spatial variations of interlayer spacings due to insufficient flatness of grating layers.

The effect of smearing transmission peaks arises also due to the limited beam width in the MM-wave experiments with multilayer structures [36, 37] when Gaussian beams are created by optical components such as lenses [41]. The effect can further be enhanced due to self-emerging instability and fracturing of shape of higher-order modes under the resonant conditions [38, 42].

7. CONCLUSIONS

We have numerically simulated multilayer grid polarizers produced with photolithographic technology for MM wave applications in the frequency range of $f = 10$–$250\,\text{GHz}$. The polarizers have been made as free-standing (free of lossy and reflective dielectric substrates) quasioptical strip-grating assemblies where gratings are specified by the period $p = 0.60\,\text{mm}$, strip width $w = 0.17\,\text{mm}$, and thickness $t = 0.10\,\text{mm}$.

Multilayer grid structures show bandwise operation where the frequency bands of enhanced polarizing performance, i.e., reduced transmission for the waves of rejected polarization as compared to the allowed one, are separated by transmission peaks for the waves of rejected polarization. Within spectral bands of enhanced performance, the structures show the polarization extinction ratio which grows in decibels approximately in proportion to the number of layers.

With one-, two-, three-layer structures at the frequencies of, e.g., $f_a = 80$–$90\,\text{GHz}$ and $f_b = 105$–$115\,\text{GHz}$ laying within the enhanced operation bands at the chosen interlayer spacing $b = 6.0\,\text{mm}$ one can reduce the rejected polarization signal to the level below $P_1 \sim -17\ldots-15\,\text{dB}$, $P_2 \sim -40\ldots-35\,\text{dB}$, $P_3 \sim -60\ldots-53\,\text{dB}$, respectively. Increasing the number of layers improves the polarizing performance until the imperfections of gratings would hamper the effect significantly due to increasing the noisy components of spectral curves.

With a single grating, the same level as P_2 can only be achieved with much finer structures having,

e.g., $w = 0.01\,\text{mm}$ and $p = 0.04\,\text{mm}$ (that means, in fact, 10 μm tungsten wire grids). As for the level of P_3, it cannot be achieved with a single free-standing metallic grating at the given frequencies, since it requires the wire diameter $w \sim 1\,\mu\text{m}$ at about the same p/w ratio, which is unrealistic to implement (besides, the skin depth in this case is, typically, $\delta \sim 0.5\,\mu\text{m}$).

Full-wave simulations of multilayer polarizers have been compared with three asymptotic models. The models use asymptotic solutions for subwavelength strip gratings and wire grids, and regularization-based solutions for strip gratings, respectively. Full-wave simulations are well reproduced by asymptotic models when the latter are specified by the sets of adjusted grating parameters.

When measured with broadband detectors of finite though small bandwidth, transmission spectra of rejected polarization show reduced peaks of resonant transparency, yet the same growth of polarizing performance between peaks. At the detector bandwidth exceeding the spectral distance between the peaks, the polarizing performance drops to the level close to the performance of a single grating.

Random spatial variations of interlayer spacings reduce the enhancement of polarizing performance, yet the latter continues to grow in proportion to the number of grating layers.

ACKNOWLEDGMENT

The work was partially supported by The Scientific and Technological Research Council of Turkey (TUBITAK) through the 2221 Fellowship Program for Visiting Scientists and Scientists on Sabbatical Leave (2019/6).

REFERENCES

1. Schott, J. R., *Fundamentals of Polarimetric Remote Sensing*, Vol. 81, SPIE Press, 2009.
2. Ryzhkov, A. V. and D. S. Zrnic, *Radar Polarimetry for Weather Observations*, Springer Nature Switzerland AG, Cham, Switzerland, 2019.
3. Dai, H., X. Wang, H. Xie, S. Xiao, and J. Luo, *Spatial Polarization Characteristics of Radar Antenna. Analysis, Measurement and Anti-jamming Application*, Springer and National Defense Industry Press, Beijing, 2019.
4. Kuwata-Gonokami, M., "Terahertz spectroscopy: Ellipsometry and active polarization control for terahertz waves," *Terahertz Spectroscopy and Imaging*, Reiponen, K.-E., J. A. Zeitler, and M. Kuwata-Gonokami, Eds., Springer Series in Optical Sciences, Vol. 171, W. T. Rhodes, Editor-in-Chief, Springer, 2013.
5. Cheng, Y., L. Qiao, D. Zhu, Y. Wang, and Z. Zhao, "Passive polarimetric imaging of millimeter and terahertz waves for personnel security screening," *Opt. Lett.*, Vol. 46, No. 6, 1233–1236, 2021.
6. Weber, T., T. Käsebier, M. Helgert, E.-B. Kley, and A. Tünnermann, "Tungsten wire grid polarizer for applications in the DUV spectral range," *Appl. Opt.*, Vol. 51, No. 16, 3224–3227, 2012.
7. Wang, J. J., W. Zhang, Z. Deng, J. Deng, F. Liu, P. Sciortino, and L. Chen, "High-performance nanowire-grid polarizers," *Opt. Lett.*, Vol. 30, No. 2, 195–197, 2005.
8. Zhou, L. and W. Liu, "Broadband polarizing beam splitter with an embedded metal-wire nanograting," *Opt. Lett.*, Vol. 30, No. 12, 1434–1436, 2005.
9. Soares, L. L. and L. Cescato, "Metallized photoresist grating as a polarizing beam splitter," *Appl. Opt.*, Vol. 40, No. 32, 5906–5910, 2001.
10. https://www.purewavepolarizers.com/wire-grid-polarizers/10-micron-wire-far-ir-thz-polarizer [Accessed: 2021-07-02].
11. Manabe, T. and A. Murk, "Transmission and reflection characteristics of slightly irregular wire-grids with finite conductivity for arbitrary angles of incidence and grid rotation," *IEEE Trans. Anten. Propagat.*, Vol. 53, No. 1, 250–259, 2005.
12. Den Boer, J. H. W. G., G. M. W. Kroesen, W. de Zeeuw, and F. J. de Hoog, "Improved polarizer in the infrared: Two wire-grid polarizers in tandem," *Opt. Lett.*, Vol. 20, No. 7, 800–802, 1995.

13. Yu, Z., P. Deshpande, W. Wu, J. Wang, and S. Y. Chou, "Reflective polarizer based on a stacked double-layer subwavelength metal grating structure fabricated using nanoimprint lithography," *Appl. Phys. Lett.*, Vol. 77, No. 7, 927–929, 2000.
14. Ekinci, Y., H. H. Solak, C. David, and H. Sigg, "Bilayer Al wire-grids as broadband and high-performance polarizers," *Opt. Express*, Vol. 14, No. 6, 2323–2334, 2006.
15. Yurchenko, V. B. and E. V. Yurchenko, "Dual-layer frequency-selective subwavelength-grid polarizers for THz applications," *Proceedings of the 6th International Kharkov Symposium Physics and Engineering of Microwaves, MM and SubMM Waves (MSMW-07)*, 222–224, Kharkov, Ukraine, June 25–30, 2007.
16. Yurchenko, V. B., M. L. Gradziel, and J. A. Murphy, "Dual-layer grid polarizers for mm and sub-mm waves: theory and experiment," *Proceedings of the 7th International Kharkov Symposium on Physics and Engineering of Microwaves, MM, SubMM Waves and Workshop on THz Technology (MSMW-10)*, W-5, Kharkov, Ukraine, June 21–26, 2010.
17. Yurchenko, V. B., J. A. Murphy, J. Barton, J. Verheggen, and K. Rodgers, "Dual-layer frequency-selective grid polarizers on thin-film substrates for THz applications," *Proceedings of the EuMW 2008: 38th European Microwave Conference 2008 (EuMC-2008)*, 10.14–10.17, Amsterdam, The Netherlands, October 28–31, 2008.
18. Sun, L., Z.-H. Lv, W. Wu, W.-T. Liu, and J.-M. Yuan, "Double-grating polarizer for terahertz radiation with high extinction ratio," *Appl. Opt.*, Vol. 49, No. 11, 2066–2071, 2010.
19. Deng, L. Y., J. H. Teng, L. Zhang, Q. Y. Wu, H. Liu, X. H. Zhang, and S. J. Chua, "Extremely high extinction ratio terahertz broadband polarizer using bilayer subwavelength metal wire-grid structure," *Appl. Phys. Lett.*, Vol. 101, 011101, 2012.
20. Lee, Y. H., P. Peranantham, and C. K. Hwangbo, "Fabrication of a bilayer wire grid polarizer in the near infrared wavelength region by using a UV curing nanoimprinting method," *J. Korean Phys. Soc.*, Vol. 61, No. 10, 1714–1719, 2012.
21. Huang, Z., E. P. J. Parrott, H. Park, H. P. Chan, and E. Pickwell-MacPherson, "High extinction ratio and low transmission loss thin-film terahertz polarizer with a tunable bilayer metal wire-grid structure," *Opt. Lett.*, Vol. 39, No, 4, 793–796, 2014.
22. Lu, B., H. Wang, J. Shen, J. Yang, H. Mao, L. Xia, W. Zhang, G. Wang, X.-Y. Peng, and D. Wang, "A high extinction ratio THz polarizer fabricated by double-bilayer wire grid structure," *AIP Adv.*, Vol. 6, 025215, 2016.
23. Xiang, W., X. Huang, D. Li, Q. Zhou, H. Guo, and J. Li, "High extinction ratio terahertz broadband polarizer based on the aligned Ni nanowire arrays," *Opt. Lett.*, Vol. 45, No. 7, 1978–1981, 2020.
24. Lee, J.-K., B. O. Kim, J. Park, J. B. Kim, I.-S. Kang, G. Sim, J. H. Park, and H.-I. Jang, "A bilayer Al nanowire-grid polarizer integrated with an IR-cut filter," *Opt. Mat.*, Vol. 98, 109409, 2019.
25. Ferraro, A., D. C. Zografopoulos, M. Missori, M. Peccianti, R. Caputo, and R. Beccherelli, "Flexible terahertz wire grid polarizer with high extinction ratio and low loss," *Opt. Lett.*, Vol. 41, No, 9, 2009–2012, 2016.
26. Islam, M. D., J. O. Kim, Y. Ko, Z. Ku, et al., "Design of high efficient mid-wavelength infrared polarizer on ormochalc polymer," *Macromol. Mater. Eng.*, Vol. 305, 2000033, 2020.
27. Popov, E. (ed.), *Gratings: Theory and Numeric Applications*, Institut Fresnel, CNRS, AMU, Marseille, France, 2012.
28. Sirenko, Y. K. and S. Ström, Eds., *Modern Theory of Gratings*, Springer, New York, 2010.
29. https://www.pdesolutions.com [Accessed: 2021-07-02].
30. Yurchenko, V., T. Navruz, M. Ciydem, and A. Altintas, "Light-controlled polarization of mm-waves with photo-excited gratings in a resonant semiconductor slab," *Adv. Electromagnetics*, Vol. 8, No. 2, 92–100, 2019.
31. Wainstein, L. A., "On the electrodynamic theory of grids. Part I, II," *Elektronika Bol'shikh Moshchnostei*, Vol. 2, 26–73, P. L. Kapitza and L. A. Wainstein, Eds., Moscow, 1963 [Engl. transl. in *High-Power Electronics*, 14–48, Pergamon Press, Oxford, 1966].

32. Agranovich, Z. S., V. A. Marchenko, and V. P. Shestopalov, "Diffraction of electromagnetic waves from plane metallic gratings," *Zhurnal Tehnicheskoy Fiziki*, Vol. 32, No. 4, 381–394, 1962 (in Russian).
33. Shestopalov, V. P., *The Method of the Riemann-Hilbert Problem in the Theory of Electromagnetic Wave Diffraction and Propagation*, Kharkov State Univ. Press, Kharkov, 1971 (in Russian).
34. Shestopalov, V. P., L. N. Litvinenko, S. A. Masalov, and V. G. Sologub, *Wave Diffraction by Gratings*, Kharkov State Univ. Press, Kharkov, 1973 (in Russian).
35. Solimeno, S., B. Crosignani, P. Di Porto, *Guiding, Diffraction, and Confinement of Optical Radiation*, Academic Press, London, 1986.
36. Yurchenko, V., M. Ciydem, M. Gradziel, J. A. Murphy, and A. Altintas, "Light-controlled photonics-based mm-wave beam switch," *Opt. Express*, Vol. 24, No. 15, 16471, 2016.
37. Yurchenko, V., M. Ciydem, M. Gradziel, and L. Yurchenko, "MM-wave dielectric parameters of magnesium fluoride glass wafers," *Progress In Electromagnetics Research M*, Vol. 62, 89–98, 2017.
38. Yurchenko, V., M. Ciydem, M. Gradziel, and J. A. Murphy, "Major reshaping of narrow beams by resonant multilayer structures," *Opt. Express*, Vol. 28, No. 6, 8211, 2020.
39. Soriano, G., M. Zerrad, and C. Amra, "Anti-scattering effect analyzed with exact theory of light scattering from rough multilayers," *Opt. Lett.*, Vol. 44, No. 18, 4455, 2019.
40. Rytov, S. M., Y. A. Kravtsov, and V. I. Tatarskii, *Principles of Statistical Radiophysics 4: Wave Propagation Through Random Media*, Springer-Verlag, Berlin, 1987.
41. Yurchenko, V. B., M. Ciydem, M. Gradziel, J. A. Murphy, and A. Altintas, "Double-sided split-step mm-wave Fresnel lenses: Design, fabrication and focal field measurements," *J. Europ. Opt. Soc. Rap. Publ.*, Vol. 9, 14007, 2014.
42. Yurchenko, V. B., A. Altintas, M. Ciydem, and S. Koc, "Experimental conditions for the excitation of thin disk whispering-gallery-mode resonators," *Progress In Electromagnetics Research C*, Vol. 43, 29–40, 2013.